Unexpected quenching effect on new particle formation from the atmospheric reaction of methanol with SO_3

Ling Liu[a,b,1], Jie Zhong[b,c,d,1], Hanna Vehkamäki[e], Theo Kurtén[f], Lin Du[g], Xiuhui Zhang[a,2], Joseph S. Francisco[b,c,d,2], and Xiao Cheng Zeng[b,2]

[a]Key Laboratory of Cluster Science, Ministry of Education of China, School of Chemistry and Chemical Engineering, Beijing Institute of Technology, 100081 Beijing, China; [b]Department of Chemistry, University of Nebraska–Lincoln, Lincoln, NE 68588; [c]Department of Earth and Environmental Sciences, University of Pennsylvania, Philadelphia, PA 19104; [d]Department of Chemistry, University of Pennsylvania, Philadelphia, PA 19104; [e]Faculty of Science, Institute for Atmospheric and Earth System Research/Physics, University of Helsinki, FI-00014 Helsinki, Finland; [f]Department of Chemistry, University of Helsinki, FI-00014 Helsinki, Finland; and [g]Environment Research Institute, Shandong University, 266237 Qingdao, China

Contributed by Joseph S. Francisco, October 18, 2019 (sent for review September 11, 2019; reviewed by Henry F. Schaefer III and Veronica Vaida)

Despite the high abundance in the atmosphere, alcohols in general and methanol in particular are believed to play a small role in atmospheric new particle formation (NPF) largely due to the weak binding abilities of alcohols with the major nucleation precursors, e.g., sulfuric acid (SA) and dimethylamine (DMA). Herein, we identify a catalytic reaction that was previously overlooked, namely, the reaction between methanol and SO_3, catalyzed by SA, DMA, or water. We found that alcohols can have unexpected quenching effects on the NPF process, particularly in dry and highly polluted regions with high concentrations of alcohols. Specifically, the catalytic reaction between methanol and SO_3 can convert methanol into a less-volatile species—methyl hydrogen sulfate (MHS). The latter was initially thought to be a good nucleation agent for NPF. However, our simulation results suggest that the formation of MHS consumes an appreciable amount of atmospheric SO_3, disfavoring further reactions of SO_3 with H_2O. Indeed, we found that MHS formation can cause a reduction of SA concentration up to 87%, whereas the nucleation ability of MHS toward new particles is not as good as that of SA. Hence, a high abundance of methanol in the atmosphere can lower the particle nucleation rate by as much as two orders of magnitude. Such a quenching effect suggests that the recently identified catalytic reactions between alcohols and SO_3 need to be considered in atmospheric modeling in order to predict SA concentration from SO_2, while also account for their potentially negative effect on NPF.

atmospheric aerosol | alcohols | SO_3 | catalytic reactions | nucleation precursors

Numerous species have been shown to participate in the formation of new atmospheric aerosol particles from vapor via nucleation. However, the prevailing nucleation mechanisms often underestimate the rates of new particle formation (NPF) (1–3), suggesting that there are still many unidentified nucleating species in the atmosphere, as well as undiscovered nucleation mechanisms. Alcohols, which are released by plants, biomass combustion, and industrial emission, are abundant in the troposphere (4–9). However, their contribution to NPF was thought to be negligible due to weak hydrogen-bonding interactions (10–12) between alcohol molecules and known important nucleation precursors such as sulfuric acid (SA) and dimethylamine (DMA) (13, 14).

Many recent studies have suggested that atmospheric species generated from gas-phase chemical reactions can play an important role in the NPF process (15–19). Alcohols are active species in the atmosphere, and they can be involved in many chemical reactions (20–22). Shen et al. (23) showed fluorescence evidence that methanol (MO) can react with SO_3 with a relatively high rate constant, although the reactant concentrations used in the laboratory were much higher than those in the ambient environment, while little water was present in the experiment. The reaction between MO and SO_3 has received increasing attention recently due to two reasons: 1) A product of the reaction—methyl hydrogen sulfate (MHS)—is less volatile than MO, which may stabilize the atmospheric clusters and promote NPF (23, 24). 2) The reaction can cause appreciable consumption of SO_3, which would lower the abundance of SA [produced via the reaction of SO_3 with H_2O (25–28)] in the atmosphere. Since SA is the most important nucleation precursor, lower SA concentration would have an impact on the nucleation rate. Such a quenching effect originating from specific atmospheric reactions was recently recognized as a key factor influencing the number of aerosol particles, as shown from measured mixtures of atmospheric vapors (2). Hence, the reaction between SO_3 and MO may play either a positive or a negative role in NPF, depending on the relative importance of the two opposing effects elucidated above. Besides the potential implications on NPF, the MHS produced by the reaction of MO with SO_3 can have negative health effects, e.g., irritating eyes and the upper respiratory tract.

Significance

New particle formation (NPF) is an important global phenomenon, contributing nearly half of the cloud condensation nuclei in nature. Today, NPF is believed to be mainly promoted by low-volatile species formed in atmosphere. Herein, we show that in certain cases, the formation of low-volatile species could undermine NPF. Specifically, we identify previously unreported catalytic reactions between alcohols and SO_3 which yield low-volatile organic sulfates. Rather than being a promoter to NPF, the low-volatile organic sulfates can compete for consuming SO_3, thereby disfavoring H_2SO_4 formation. Such unexpected quenching effects on NPF are most likely to occur in dry and polluted regions with abundant alcohols, illustrating the importance in understanding the interplay between nucleation precursor formation and subsequent NPF.

Author contributions: L.L., J.Z., X.Z., J.S.F., and X.C.Z. designed research; L.L. and J.Z. performed research; X.Z., J.S.F., and X.C.Z. contributed new reagents/analytic tools; L.L., J.Z., H.V., T.K., L.D., X.Z., J.S.F., and X.C.Z. analyzed data; and L.L., J.Z., X.Z., J.S.F., and X.C.Z. wrote the paper.

Reviewers: H.F.S., University of Georgia; and V.V., University of Colorado.

The authors declare no competing interest.

[1]L.L. and J.Z. contributed equally to this work.

[2]To whom correspondence may be addressed. Email: zhangxiuhui@bit.edu.cn, frjoseph@sas.upenn.edu, or xzeng1@unl.edu.

This article contains supporting information online at https://www.pnas.org/lookup/suppl/doi:10.1073/pnas.1915459116/-/DCSupplemental.

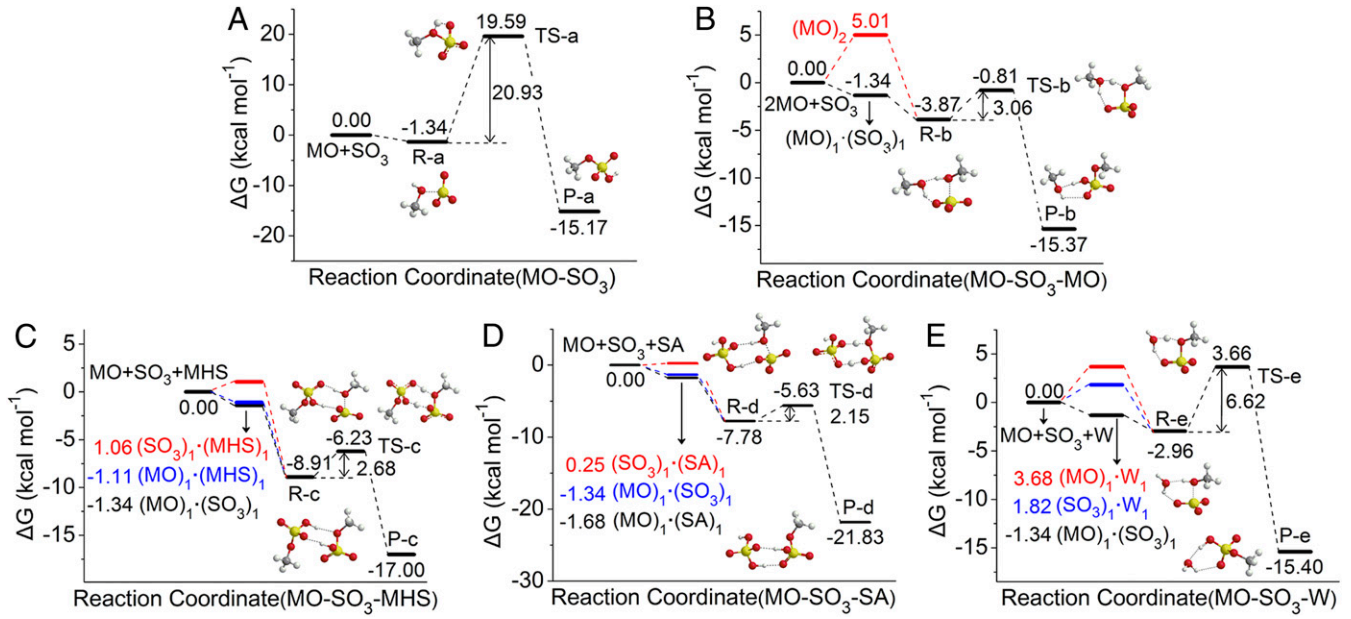

Fig. 1. Gibbs free-energy (in kcal mol^{-1} at 298.15 K) profiles for the gas-phase reaction of MO and SO_3 at the CCSD(T)-F12/cc-pVDZ-F12//M06-2X/6–311++G(3df,3pd) level of theory. (*A*) uncatalyzed, (*B*) MO-catalyzed, (*C*) MHS-catalyzed, (*D*) SA-catalyzed, and (*E*) H_2O (W)-catalyzed gas-phase reaction between MO and SO_3. The structures of the corresponding reactants (R), transition states (TSs), and products (P) are also shown. The gray, white, red, and yellow balls represent C, H, O, and S atoms, respectively.

Currently, emissions from power plants is considered the primary source of MHS (29), although secondary sources are less explored. In addition to detection near power plants, MHS is also widely detected near city freeways (30), as well as in rural areas (31), with atmospheric concentration reaching up to 5.0×10^7 molecules cm^{-3}. For example, during the smog episode in Los Angeles (32), very high atmospheric concentration of MHS of up to 1.1×10^{11} molecules cm^{-3} was reported. Hence, exploration of the atmospheric secondary source of MHS and the role of chemical formation of MHS in NPF is of fundamental importance. An improved understanding of the MO–SO_3 reaction and the corresponding chemical formation mechanism of MHS are also important to assess the effects of abundant small alcohols on NPF. Here, the MO–SO_3 reaction in the ambient condition was studied by using high-level density-functional theory and Born–Oppenheimer molecular-dynamics simulations. In addition, the combined effects of this reaction and the subsequent nucleation process are evaluated using the Atmospheric Cluster Dynamics Code (ACDC) (33, 34).

Results and Discussion

Reaction Mechanism of MO with SO_3. The gas-phase MO–SO_3 reaction is investigated at the coupled cluster with singles, doubles, and perturbative triples [CCSD(T)]-F12/cc-pVDZ-F12//M06-2X/6–311++G(3df,3pd) level of theory. In the presumed reaction (without catalyst) of MO–SO_3 (Fig. 1*A*), the oxygen atom of MO can react with the sulfur atom of SO_3 to form an ester, followed by simultaneous proton transfers from MO to SO_3. The Gibbs free-energy barrier of this reaction is 20.93 kcal mol^{-1}, while the corresponding effective rate coefficient (1.20×10^{-19} cm^3 molecule^{-1} s^{-1}, see *SI Appendix*, Table S1) is approximately six orders of magnitude lower than the value measured experimentally [$(1.17 \pm 0.16) \times 10^{-13}$ cm^3 molecule^{-1} s^{-1}, 295 ± 2 K) (23)], indicating that a direct reaction between MO and SO_3 is unlikely to occur under atmospheric conditions.

Notably, the hydroxyl group of the reactant MO and the sulfate ester group of the product (MHS) can act as both hydrogen-atom donors and -acceptors to promote proton transfer, suggesting that MO and MHS may be able to catalyze the MO–SO_3 reaction. As shown in the computed energy profiles (Fig. 1 *B* and *C*), the free-energy barriers of the reactions with either catalyst are lowered significantly, to 3.06 kcal mol^{-1} (MO) and 2.68 kcal mol^{-1} (MHS), respectively. Under the experimental concentrations ([MO] = 4.3×10^{14} molecules cm^{-3}, [SO_3] = 3×10^{12} molecules cm^{-3}), the effective rate coefficient for the MO-catalyzed reaction is 5.23×10^{-12} cm^3 molecule^{-1} s^{-1}, which is close to the experimental value of 1.17×10^{-13} cm^3 molecule^{-1} s^{-1}. This result thus explains the experimental findings and provides a possible reaction pathway for the MO–SO_3 in the atmosphere. The details of the effective rate coefficient for the MHS catalyzed reaction are shown in *SI Appendix*, Part 1 and Table S1.

Important common atmospheric species (SA, DMA, and H_2O) have been detected in the atmosphere (14). These species can also act as relatively strong hydrogen-atom donors/acceptors, thereby promoting various proton transfer reactions (35, 36), and possibly catalyzing the MO–SO_3 reaction. Therefore, the catalytic effects of SA/DMA/H_2O on the MO–SO_3 reaction were also investigated. As shown in Fig. 1*D*, the free-energy barrier of the reaction catalyzed by SA is 2.15 kcal mol^{-1}, which is even lower

Table 1. Concentrations of the catalysts ([M], molecules cm^{-3}), the effective reaction rate coefficients (k_{eff}, cm^3 molecule^{-1} s^{-1}), and the reaction rates (v, molecules cm^{-3} s^{-1}) for the formation of MHS from the MO–SO_3 reaction catalyzed by M (M = SA, DMA, or H_2O) calculated at the CCSD(T)-F12/cc-pVDZ-F12//M06-2X/6–311++G(3df,3pd) level of theory and at 298.15 K

M	[M], molecules cm^{-3}	k_{eff}, cm^3 molecule^{-1} s^{-1}	v, molecules cm^{-3} s^{-1}
Uncatalyzed	—	1.20×10^{-19}	1.20×10^{-3}
SA	1.0×10^7	9.42×10^{-20}	9.42×10^{-4}
DMA	1.0×10^9	2.47×10^{-14}	2.47×10^2
H_2O	1.0×10^{15}	8.50×10^{-12}	8.50×10^4

[SO_3] = 1.0×10^3 molecules cm^{-3}, [MO] = 1.0×10^{13} molecules cm^{-3}.

than that with MO or MHS as catalysts. The reaction catalyzed by DMA is expected to be barrierless since our Born–Oppenheimer molecular-dynamics (BOMD) simulation shows that the MO–SO_3 reaction catalyzed by DMA (*SI Appendix*, Fig. S1*A*) can occur in approximately 1 ps. Lastly, the Gibbs free-energy barrier for the H_2O-catalyzed MO–SO_3 reaction is 6.62 kcal mol^{-1}. Since the atmospheric concentration of H_2O is several orders of magnitudes higher than that of SA or DMA, the MO–SO_3 reaction catalyzed by H_2O may still be appreciable despite its relatively high free-energy barrier.

As shown in Table 1, H_2O is actually the most effective catalyst for the MO–SO_3 reaction. Furthermore, the rate of the MO–SO_3 reaction catalyzed by H_2O is comparable to that of the H_2O–SO_3 reaction (commonly viewed as the dominant pathway by which SO_3 is consumed), especially under relatively dry (e.g., winter) and highly polluted conditions with low H_2O concentrations and high MO concentrations (see the yellow and red areas in Fig. 2, and more details are shown in *SI Appendix*, Part 2 and Tables S2–S4). Overall, the MO–SO_3 reaction can be viewed as an important secondary source of atmospheric MHS.

Note that gas-phase reactions catalyzed by water molecules in the atmosphere is frequently proposed in the literature (27, 37–40). However, the equilibrium constants of hydrate formation between most potential reactant molecules and water (37) are usually very low due to their low binding energies, rendering the catalytic gas-phase reactions unimportant in the atmosphere. SO_3 is an exception due to its high water affinity. Indeed, many gas-phase reactions involving SO_3 can be efficiently catalyzed by water (27, 38).

Note also that the reactions between SO_3 and other important atmospheric species bearing alcoholic hydroxyl groups, such as ethanol, glycolaldehyde, isopropanol, and glycolic acid, are also studied (*SI Appendix*, Table S5 and Fig. S2). The Gibbs free-energy barriers of these H_2O-catalyzed reactions are in the range of 4.54 to 7.24 kcal/mol, and these energy-barrier values are close to that of the H_2O-catalyzed MO–SO_3 reaction. Hence, the identified reaction mechanism with SO_3 appears to be a general one and can be applicable to other species with alcoholic hydroxyl groups.

Opposing Roles of MO–SO_3 Reaction in the Nucleation Process. The above calculations show that the MO–SO_3 reaction could feasibly occur under the catalysis of H_2O, which might be an important secondary source of MHS in the atmosphere. Since the produced MHS can form stronger hydrogen bonds than the reactant MO (see the molecular electrostatic potential analysis in *SI Appendix*, Part 3 and Fig. S3), and the atom-in-molecule topological analysis for the most stable clusters involving MHS shows that MHS can form relatively strong hydrogen bond with SA and DMA (*SI Appendix*, Part 4 and Table S6), the MO–SO_3 reaction may have implications for atmospheric aerosol nucleation. In many previous studies, chemical reactions involved in nucleation precursor formation and the subsequent nucleation process are usually considered and modeled as two independent stages. If the competitive chemical reactions that are involved in nucleation precursor formation are not considered, the concentrations of the precursors would be constant, for example, the concentration of SA. In this scenario, the participation of MHS into SA-DMA–based NPF would enhance the particle formation rate (*SI Appendix*, Fig. S4), a prediction similar to the previously reported enhancement effect of SFA on SA-DMA–based NPF (41). However, if the chemical reactions involved in nucleation precursor formation are considered, the MO–SO_3 reaction effectively competes with the H_2O–SO_3 reaction for consuming SO_3, thus lowering the concentration of SA in atmosphere.

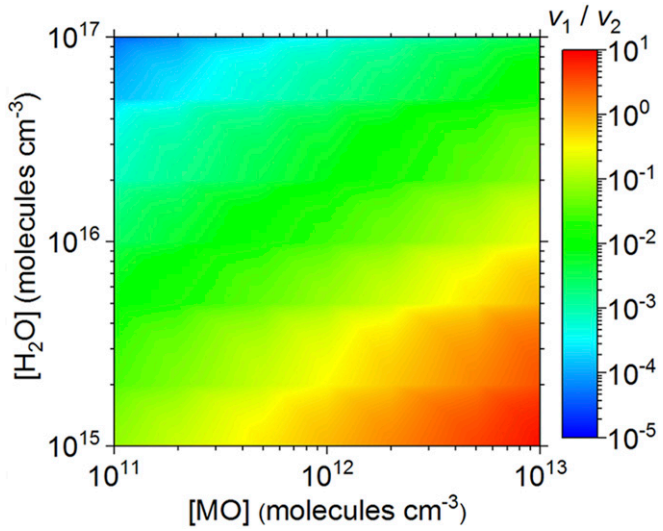

Fig. 2. Ratios of reaction rates (v_1/v_2) for the MO–SO_3 reaction catalyzed by H_2O (v_1) and the H_2O–SO_3 reaction catalyzed by H_2O (v_2) at varying MO and H_2O concentrations ([MO], [H_2O], molecules cm^{-3}) in the atmospheric concentration range.

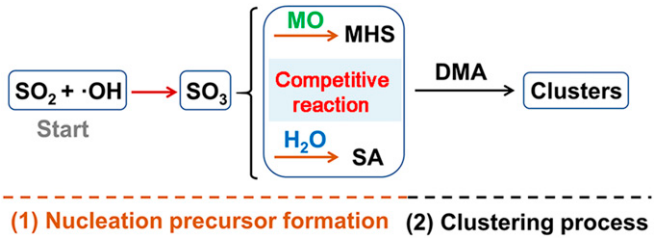

Fig. 3. Simulated processes. The brown arrows represent the competitive nucleation precursor formation processes, and the black arrow represents the clustering process.

The decrease in the SA concentration and the clustering processes involving MHS need to be simultaneously modeled in order to understand the realistic role of the MO–SO_3 reaction in atmospheric nucleation. To this end, the combined process was simulated (Fig. 3; further details are given Part 5 in *SI Appendix*): 1) The competitive chemical reactions involved in the formation of potential nucleation precursors (MHS formation from the MO–SO_3 reaction and SA formation from H_2O–SO_3 reaction), and 2) the subsequent clustering process involving MHS, SA, and DMA. Since accurate atmospheric concentration of SO_3 is still unclear due to the highly reactive nature of SO_3, the simulated system starts from the reaction between SO_2 and ·OH (*SI Appendix*, Fig. S5 and Table S7), providing a constant source of SO_3 (*SI Appendix*, Fig. S6) for accurately evaluating the competing formation of MHS and SA.

As shown in Fig. 4, at moderate atmospheric concentrations of SO_2 (5.0×10^{10} molecules cm^{-3}) and ·OH (5.0×10^{6} molecules cm^{-3}) (42–45), the presence of MO up to 1.0×10^{13} molecules cm^{-3} [i.e., abundant MO in highly polluted regions (7, 9)] can produce significant amounts of MHS, but simultaneously suppresses SA production by 21~87% as [H_2O] varies from 1.0×10^{16} to 1.0×10^{15} molecules cm^{-3}, corresponding to relatively dry regions (*SI Appendix*, Table S8). The SA concentration is almost unaffected by the presence of MO in relatively humid areas for [H_2O] > 1.0×10^{16} molecules cm^{-3} (*SI Appendix*, Fig. S7). The degree of [SA] reduction with the increase of MO concentration is approximately equal at different concentrations of SO_2 and ·OH (*SI Appendix*, Fig. S8). Therefore, the influence on SA concentration is important only in dry and polluted areas. It is noteworthy that in practical applications, the SA concentration is often directly predicted from SO_2 concentrations (44, 46), without accounting for other

CHEMISTRY

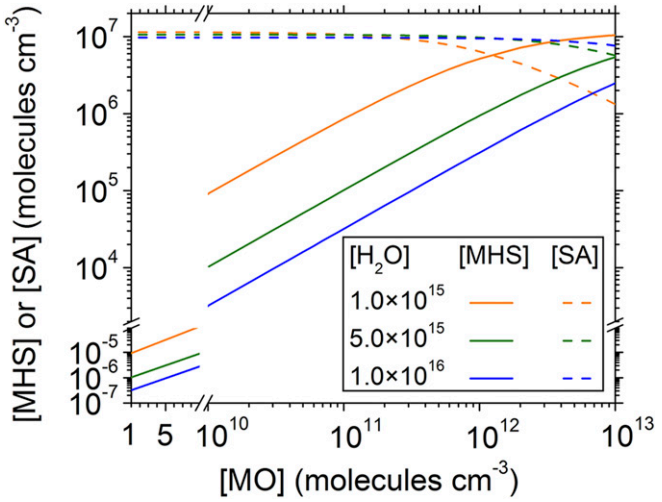

Fig. 4. MHS concentration ([MHS], solid lines) and SA concentration ([SA], dashed lines) (molecules cm^{-3}) predicted when accounting for both the MO–SO_3 reaction and the H_2O–SO_3 reaction at different H_2O concentrations ([H_2O], 1.0×10^{15}, 5.0×10^{15}, and 1.0×10^{16} molecules cm^{-3}) versus the MO concentration at 280 K. [SO_2] = 5.0×10^{10} molecules cm^{-3} and [·OH] = 5.0×10^6 molecules cm^{-3}.

reactions competing for SO_3. Hence, taking the competing MO–SO_3 reaction into account in such calculations would improve the prediction of the SA concentrations.

Although MHS can enhance the rate of SA-DMA–based NPF, the formation reaction of MHS can also decrease the concentration of the most important nucleation precursor, SA. As such, the effects of the MO–SO_3 reaction on the particle nucleation rate (J) were further investigated by considering simultaneously the relevant formation reactions (SO_2··OH, MO–SO_3, H_2O–SO_3), and the subsequent clustering process, under the realistic atmospheric concentrations and temperature. As shown in Fig. 5*A*, J decreases by up to two orders of magnitude as [MO] increases from 1.0×10^{10} molecules cm^{-3} to 1.0×10^{13} molecules cm^{-3} (within the range of atmospheric concentrations) (4–9). The reduction in J can be attributed to the [SA] reduction, and to the fact that MHS has a weaker ability to form hydrogen bond compared to SA, as illustrated by the molecular electrostatic potential analysis (*SI Appendix*, Part 3 and Fig. S3). Fig. 5*B* shows the nucleation rate when the sum ([SA]+[MHS]) is kept constant. Again, J decreases as the ratio of the MHS concentration to the sum of [SA] and [MHS] (i.e., [MHS]/([SA]+[MHS])) increases, which further indicates that MHS is a relatively weaker nucleation precursor than SA.

As shown in *SI Appendix*, Fig. S9, the number concentration of large clusters containing MHS and DMA molecules is approximately one order of magnitude lower than that of large clusters containing SA and DMA molecules. In addition, when comparing clusters with the same numbers of acid molecules and the same numbers of base molecules (with MHS counted as an acid), the Gibbs free energies of formation and evaporation rates (*SI Appendix*, Table S9) for most of clusters including MHS ($(SA)_m$·$(DMA)_n$·$(MHS)_l$, $0 \le m + l \le 3$, and $0 \le n \le m + l$) are higher than those of the corresponding pure SA-DMA–based clusters [$(SA)_{m+l}$·$(DMA)_n$, $0 \le m + l \le 3$, and $0 \le n \le m + l$], also indicating that the stabilities of most clusters including MHS are lower than those of pure SA-DMA–based clusters. As a result, the nucleation promoted by MHS (MO–SO_3) cannot offset the nucleation suppressed by the [SA] reduction (H_2O–SO_3). Therefore, the competitive formation reactions of nucleation precursors under atmospheric conditions (concentration and temperature) need to be considered when evaluating their overall roles in nucleation events.

To our knowledge, MHS is one case where competing formation reactions of nucleation precursors show a marked quenching effect on NPF. Other sulfates formed from atmospheric abundant and larger species with alcoholic hydroxyl groups and many other functional groups tend to be much less volatile than H_2SO_4, and thus could potentially promote rather than quench the NPF. In our previous study of the formation of SFA (due to NH_3–SO_3 reaction) on NPF, the competitive formation of SFA and SA were not considered (41) because the quenching effects of the NH_3–SO_3 reaction on the SA concentration and the SA-DMA particle formation rate are negligible (*SI Appendix*, Tables S10 and S11). In other words, not every competitive formation process of precursor has a strong quenching effect on SA-DMA–based atmospheric aerosol nucleation—the presence or absence of quenching depends on the details of the concentrations and properties of the relevant chemical species under the realistic atmospheric conditions.

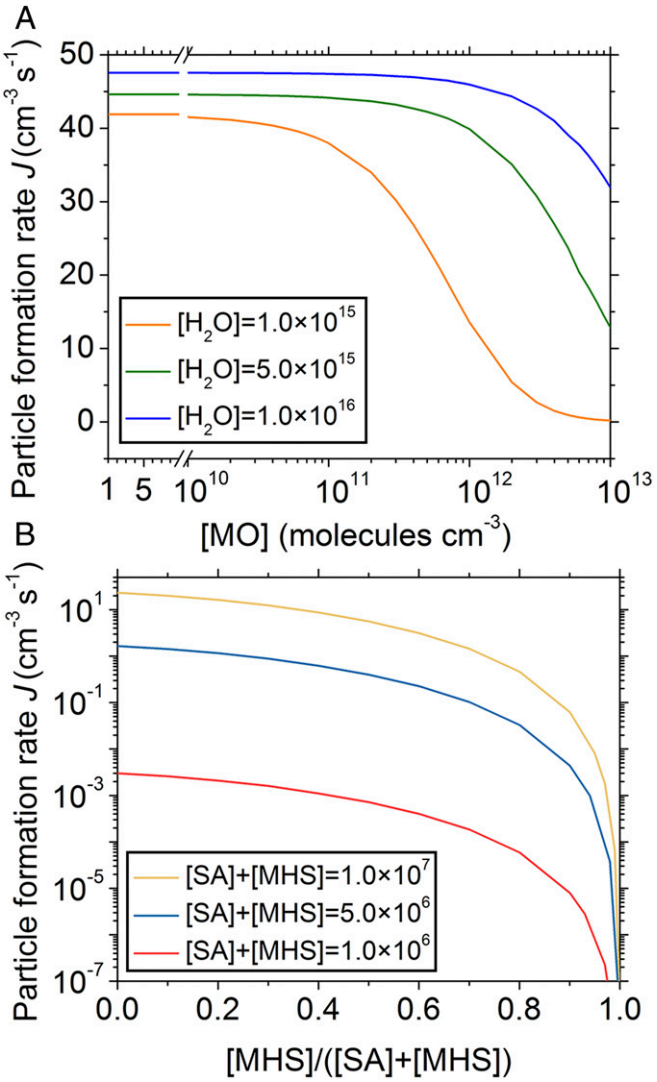

Fig. 5. Particle formation rates (J, cm^{-3} s^{-1}). (*A*) J with varying MO concentrations under different H_2O concentrations (1.0×10^{15}, 5.0×10^{15}, and 1.0×10^{16} molecules cm^{-3}) at 280 K. [DMA] = 1.0×10^9 molecules cm^{-3}, [SO_2] = 5.0×10^{10} molecules cm^{-3}, and [·OH] = 5.0×10^6 molecules cm^{-3}. (*B*) J with varying ratios of [MHS]/([SA] + [MHS]) at 280 K. [DMA] = 1.0×10^9 molecules cm^{-3}, [SA] + [MHS] = 1.0×10^7 molecules cm^{-3}.

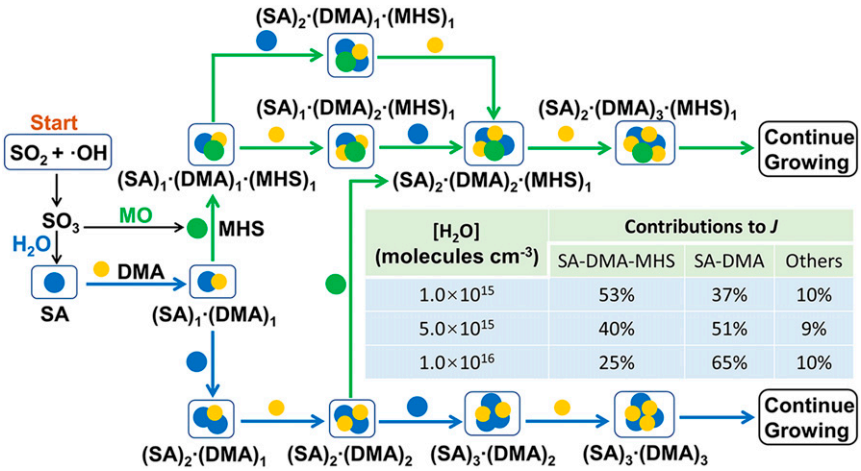

[H_2O] (molecules cm^{-3})	Contributions to J		
	SA-DMA-MHS	SA-DMA	Others
1.0×10^{15}	53%	37%	10%
5.0×10^{15}	40%	51%	9%
1.0×10^{16}	25%	65%	10%

Fig. 6. Main formation pathways of clusters at 280 K. The green arrows represent the SA-DMA-MHS nucleation pathway, and the blue arrows represent the SA-DMA nucleation pathway. [DMA] = 1.0×10^9 molecules cm^{-3}, [MO] = 1.0×10^{13} molecules cm^{-3}, [SO_2] = 5.0×10^{10} molecules cm^{-3}, and [·OH] = 5.0×10^6 molecules cm^{-3}. The contributions to particle formation rates (J, cm^{-3} s^{-1}) at different H_2O concentrations are indicated in the inset table.

Nucleation Mechanism of SA-DMA-MHS–Based Clusters. Finally, the nucleation mechanism of SA-DMA-MHS–based clusters at different [H_2O] is investigated (details are shown in Part 3 of *SI Appendix*). As shown in Fig. 6, MO can compete with H_2O for SO_3 to form MHS. Overall, the nucleation involves two pathways: 1) The SA-DMA nucleation pathway and 2) the SA-DMA-MHS nucleation pathway. In both pathways, the $(SA)_1{\cdot}(DMA)_1$ cluster is initially formed from monomers of SA and DMA. In the SA-DMA nucleation pathway (blue arrows), SA-DMA clusters grow by the stepwise addition of either SA or DMA, as shown in previous studies (41, 47). In the SA-DMA-MHS nucleation pathway (green arrows), MHS combines with the $(SA)_1{\cdot}(DMA)_1$ cluster first, and then this cluster grows by the stepwise addition of SA or DMA. In addition, MHS can also combine with a larger $(SA)_2{\cdot}(DMA)_2$ cluster. As shown in the inset table of Fig. 6, the SA-DMA-MHS pathway contributes to overall particle formation by 25% at [H_2O] = 1.0×10^{16} molecules cm^{-3} and by 53% at lower [H_2O] = 1.0×10^{15} molecules cm^{-3}. Therefore, the effect of MHS becomes remarkable in dry and polluted areas with relatively low H_2O concentration and high MO concentration, e.g., in winter in northern China. In such conditions, the extensive participation of MHS in the nucleation of atmospheric aerosol may have serious environmental effects.

Conclusion

In conclusion, we identified a catalytic reaction that was previously overlooked in the atmosphere, namely, the chemical reaction between methanol and SO_3, catalyzed by SA, DMA, and water molecules. This reaction leads to the gas-phase formation of MHS, thereby providing a potential secondary source of MHS in the atmosphere. The possible strong quenching effect of methanol on atmospheric nucleation, especially in dry areas with relatively high concentrations of alcohols, is also reported. We show that MHS can play two opposing roles in NPF: the quenching effect due to competing formation reactions of nucleation precursors and the promotion of the subsequent nucleation processes. In either case, both MHS itself and the active participation of MHS in atmospheric aerosol nucleation can be harmful to human health. Finally, the identified reaction mechanism with SO_3 appears to be generalizable to other species involving alcoholic hydroxyl groups. Considering the two opposing effects of these reactions with SO_3 may be important not only to accurately predict SA concentrations from the source of SO_2 but also to model the effect of these species on atmospheric NPF.

Methods

The molecular structures of the reactants, products, and the transition states (TSs) were all optimized using the M06-2X (48, 49) functional with the 6–311++G(3df,3pd) (50) basis set. The vibrational frequencies were calculated to confirm the absence of imaginary frequencies in all stable structures, and the TSs possess only one imaginary frequency (*SI Appendix*, Table S12). In addition, to confirm that each TS connects the reactant to the corresponding product, intrinsic reaction coordinate calculations were performed. Single-point energy calculations were carried out at the CCSD(T)-F12/cc-pVDZ-F12 (51–53) level of theory based on the optimized geometries at the M06-2X/6–311++G(3df,3pd) level of theory using the ORCA 3.0.3 program package (54, 55). Detailed calculations regarding the effective reaction rate coefficients are shown in Part 1 of *SI Appendix*. Details of BOMD simulations are given in Part 6 of *SI Appendix*.

To search for the lowest-energy structures of the clusters considered, the ABCluster (56, 57) program was employed to generate initially guess structures. Combinations of different levels of theory was used to further optimize the structures (see details in Part 6 and *SI Appendix*, Fig. S10 and Table S13). All of the quantum-chemistry calculations were carried out with the Gaussian 09 (revision A.01) program package (58).

The ACDC (33, 34) was used to simulate the cluster formation process with structural, thermodynamic, and kinetic data generated by quantum-chemistry calculations as the inputs. The time dependence of the concentration of each cluster was determined by integrating the birth–death equations (33) numerically using the ode15s solver in the MATLAB-R2013a program (59) (see details in Part 6 of *SI Appendix*).

Data Availability. All data are available in the manuscript and in *SI Appendix*.

ACKNOWLEDGMENTS. X.Z. and L.D. are indebted to the National Natural Science Foundation of China (Grants 21976015 and 91644214) for the support of this research. L.L. thanks China Scholarship Council. T.K. thanks the Academy of Finland for funding. H.V. thanks the European Research Council (Grant 692891-DAMOCLES) and the University of Helsinki, Faculty of Science ATMATH project for funding. J.S.F. and X.C.Z. acknowledge the computation support of University of Nebraska Holland Computing Center.

1. F. Bianchi *et al.*, Highly oxygenated organic molecules (HOM) from gas-phase autoxidation involving peroxy radicals: A key contributor to atmospheric aerosol. *Chem. Rev.* **119**, 3472–3509 (2019).
2. G. McFiggans *et al.*, Secondary organic aerosol reduced by mixture of atmospheric vapours. *Nature* **565**, 587–593 (2019).
3. C. L. Heald *et al.*, A large organic aerosol source in the free troposphere missing from current models. *Geophys. Res. Lett.* **32**, 1–4 (2005).
4. H. A. Scheeren *et al.*, The impact of Monsoon outflow from India and Southeast Asia in the upper troposphere over the eastern Mediterranean. *Atmos. Chem. Phys.* **3**, 1589–1608 (2003).

5. H. B. Singh, M. Kanakidou, P. J. Crutzen, D. J. Jacob, High concentrations and photochemical fate of oxygenated hydrocarbons in the global troposphere. *Nature* **378**, 50–54 (1995).
6. A. Mellouki, T. J. Wallington, J. Chen, Atmospheric chemistry of oxygenated volatile organic compounds: Impacts on air quality and climate. *Chem. Rev.* **115**, 3984–4014 (2015).
7. B. G. Heikes *et al*., Atmospheric methanol budget and ocean implication. *Global Biogeochem. Cycles* **16**, 1133 (2002).
8. H. Singh *et al*., Evidence from the Pacific troposphere for large global sources of oxygenated organic compounds. *Nature* **410**, 1078–1081 (2001).
9. T. J. Kelly, P. J. Callahan, J. Pleil, G. F. Evans, Method development and field measurements for polar volatile organic compounds in ambient air. *Environ. Sci. Technol.* **27**, 1146–1153 (1993).
10. H. Li, O. Kupiainen-Määttä, H. Zhang, X. Zhang, M. Ge, A molecular-scale study on the role of lactic acid in new particle formation: Influence of relative humidity and temperature. *Atmos. Environ.* **166**, 479–487 (2017).
11. H. Zhang *et al*., The enhancement mechanism of glycolic acid on the formation of atmospheric sulfuric acid-ammonia molecular clusters. *J. Chem. Phys.* **146**, 184308 (2017).
12. M. Rozenberg, A. Loewenschuss, C. J. Nielsen, Hydrogen bonding in the sulfuric acid-methanol-water system: A matrix isolation and computational study. *J. Phys. Chem. A* **119**, 2271–2280 (2015).
13. M. Sipilä *et al*., The role of sulfuric acid in atmospheric nucleation. *Science* **327**, 1243–1246 (2010).
14. L. Yao *et al*., Atmospheric new particle formation from sulfuric acid and amines in a Chinese megacity. *Science* **361**, 278–281 (2018).
15. R. Zhang, A. Khalizov, L. Wang, M. Hu, W. Xu, Nucleation and growth of nanoparticles in the atmosphere. *Chem. Rev.* **112**, 1957–2011 (2012).
16. L. Liu *et al*., Clustering mechanism of oxocarboxylic acids involving hydration reaction: Implications for the atmospheric models. *J. Chem. Phys.* **148**, 214303 (2018).
17. L. Wang *et al*., Atmospheric nanoparticles formed from heterogeneous reactions of organics. *Nat. Geosci.* **3**, 238–242 (2010).
18. V. Hirvonen, N. Myllys, T. Kurtén, J. Elm, Closed-shell organic compounds might form dimers at the surface of molecular clusters. *J. Phys. Chem. A* **122**, 1771–1780 (2018).
19. A. Metzger *et al*., Evidence for the role of organics in aerosol particle formation under atmospheric conditions. *Proc. Natl. Acad. Sci. U.S.A.* **107**, 6646–6651 (2010).
20. A. Mellouki, G. Le Bras, H. Sidebottom, Kinetics and mechanisms of the oxidation of oxygenated organic compounds in the gas phase. *Chem. Rev.* **103**, 5077–5096 (2003).
21. M. R. McGillen *et al*., Criegee intermediate-alcohol reactions, a potential source of functionalized hydroperoxides in the atmosphere. *ACS Earth Space Chem.* **1**, 664–672 (2017).
22. Y. H. Lin *et al*., Criegee intermediate reaction with alcohol is enhanced by a single water molecule. *J. Phys. Chem. Lett.* **9**, 7040–7044 (2018).
23. G. Shen, M. Suto, L. C. Lee, Reaction rate constant of $SO_3 + CH_3OH$ in the gas phase. *Int. J. Chem. Kinet.* **22**, 633–639 (1990).
24. X. Sheng, H. Zhao, L. Du, Molecular understanding of the interaction of methyl hydrogen sulfate with ammonia/dimethylamine/water. *Chemosphere* **186**, 331–340 (2017).
25. J. A. Phillips, M. Canagaratna, H. Goodfriend, K. R. Leopold, Microwave detection of a key intermediate in the formation of atmospheric sulfuric acid: The structure of H_2O-SO_3. *J. Phys. Chem.* **99**, 501–504 (1995).
26. D. L. Fiacco, S. W. Hunt, K. R. Leopold, Microwave investigation of sulfuric acid monohydrate. *J. Am. Chem. Soc.* **124**, 4504–4511 (2002).
27. K. Morokuma, C. Muguruma, Ab initio molecular orbital study of the mechanism of the gas phase reaction $SO_3 + H_2O$: Importance of the second water molecule. *J. Am. Chem. Soc.* **116**, 10316–10317 (1994).
28. M. Torrent-Sucarrat, J. S. Francisco, J. M. Anglada, Sulfuric acid as autocatalyst in the formation of sulfuric acid. *J. Am. Chem. Soc.* **134**, 20632–20644 (2012).
29. D. J. Eatough *et al*., Dimethyl sulfate in particulate matter from coal- and oil-fired power plants. *Environ. Sci. Technol.* **15**, 1502–1506 (1981).
30. Y. Suzuki, M. Kawakami, K. Akasaka, 1H NMR application for characterizing water-soluble organic compounds in urban atmospheric particles. *Environ. Sci. Technol.* **35**, 2656–2664 (2001).
31. A. P. S. Hettiyadura *et al*., Qualitative and quantitative analysis of atmospheric organosulfates in Centreville, Alabama. *Atmos. Chem. Phys.* **17**, 1343–1359 (2017).
32. D. J. Eatough, V. F. White, L. D. Hansen, N. L. Eatough, J. L. Cheney, Identification of gas-phase dimethyl sulfate and monoethyl sulfate in the Los Angeles atmosphere. *Environ. Sci. Technol.* **20**, 867–872 (1986).
33. M. J. McGrath *et al*., Atmospheric cluster dynamics Code: A flexible method for solution of the birth-death equations. *Atmos. Chem. Phys.* **12**, 2345–2355 (2012).
34. T. Olenius, O. Kupiainen-Määttä, I. K. Ortega, T. Kurtén, H. Vehkamäki, Free energy barrier in the growth of sulfuric acid-ammonia and sulfuric acid-dimethylamine clusters. *J. Chem. Phys.* **139**, 084312 (2013).
35. L. Liu, X. Zhang, Z. Li, Y. Zhang, M. Ge, Gas-phase hydration of glyoxylic acid: Kinetics and atmospheric implications. *Chemosphere* **186**, 430–437 (2017).
36. X. F. Tan *et al*., Atmospheric chemistry of CH_3CHO: The hydrolysis of CH_3CHO catalyzed by H_2SO_4. *Phys. Chem. Chem. Phys.* **20**, 7701–7709 (2018).
37. D. L. Thomsen *et al*., On the possible catalysis by single water molecules of gas-phase hydrogen abstraction reactions by OH radicals. *Phys. Chem. Chem. Phys.* **14**, 12992–12999 (2012).
38. J. Zhong, M. Kumar, J. S. Francisco, X. C. Zeng, Insight into chemistry on cloud/aerosol water surfaces. *Acc. Chem. Res.* **51**, 1229–1237 (2018).
39. S. R. Kumbhani *et al*., Water vapor enhancement of rates of peroxy radical reactions. *Int. J. Chem. Kinet.* **47**, 395–409 (2015).
40. L. Sheps *et al*., The reaction of criegee intermediate CH_2OO with water dimer: Primary products and atmospheric impact. *Phys. Chem. Chem. Phys.* **19**, 21970–21979 (2017).
41. H. Li *et al*., Self-catalytic reaction of SO_3 and NH_3 to produce sulfamic acid and its implication to atmospheric particle formation. *J. Am. Chem. Soc.* **140**, 11020–11028 (2018).
42. Z. Wang, F. Zheng, W. Zhang, S. Wang, Analysis of SO_2 pollution changes of Beijing-Tianjin-Hebei region over China based on OMI observations from 2006 to 2017. *Adv. Meteorol.* **2018**, 8746068 (2018).
43. F. Wu *et al*., Investigations of temporal and spatial distribution of precursors SO_2 and NO_2 vertical columns in the North China Plain using mobile DOAS. *Atmos. Chem. Phys.* **18**, 1535–1554 (2018).
44. S. Mikkonen *et al*., A statistical proxy for sulphuric acid concentration. *Atmos. Chem. Phys.* **11**, 11319–11334 (2011).
45. D. Stone, L. K. Whalley, D. E. Heard, Tropospheric OH and HO_2 radicals: Field measurements and model comparisons. *Chem. Soc. Rev.* **41**, 6348–6404 (2012).
46. Y. Lu *et al*., A proxy for atmospheric daytime gaseous sulfuric acid concentration in urban Beijing. *Atmos. Chem. Phys.* **19**, 1971–1983 (2019).
47. J. Almeida *et al*., Molecular understanding of sulphuric acid-amine particle nucleation in the atmosphere. *Nature* **502**, 359–363 (2013).
48. Y. Zhao, D. G. Truhlar, The M06 suite of density functionals for main group thermochemistry, thermochemical kinetics, noncovalent interactions, excited states, and transition elements: Two new functionals and systematic testing of four M06-class functionals and 12 other functions. *Theor. Chem. Acc.* **120**, 215–241 (2008).
49. Y. Zhao, D. G. Truhlar, Applications and validations of the Minnesota density functionals. *Chem. Phys. Lett.* **502**, 1–13 (2011).
50. M. J. Frisch, J. A. Pople, J. S. Binkley, Self-consistent molecular orbital methods 25. Supplementary functions for Gaussian basis sets. *J. Chem. Phys.* **80**, 3265–3269 (1984).
51. N. Bork, J. Elm, T. Olenius, H. Vehkamäki, Methane sulfonic acid-enhanced formation of molecular clusters of sulfuric acid and dimethyl amine. *Atmos. Chem. Phys.* **14**, 12023–12030 (2014).
52. N. Myllys, J. Elm, R. Halonen, T. Kurtén, H. Vehkamäki, Coupled cluster evaluation of the stability of atmospheric acid-base clusters with up to 10 molecules. *J. Phys. Chem. A* **120**, 621–630 (2016).
53. J. Elm, K. Kristensen, Basis set convergence of the binding energies of strongly hydrogen-bonded atmospheric clusters. *Phys. Chem. Chem. Phys.* **19**, 1122–1133 (2017).
54. K. E. Yousaf, K. A. Peterson, Optimized auxiliary basis sets for explicitly correlated methods. *J. Chem. Phys.* **129**, 184108 (2008).
55. F. Neese, The ORCA program system. *Wiley Interdiscip. Rev. Comput. Mol. Sci.* **2**, 73–78 (2012).
56. J. Zhang, M. Dolg, ABCluster: The artificial bee colony algorithm for cluster global optimization. *Phys. Chem. Chem. Phys.* **17**, 24173–24181 (2015).
57. J. Zhang, M. Dolg, Global optimization of clusters of rigid molecules using the artificial bee colony algorithm. *Phys. Chem. Chem. Phys.* **18**, 3003–3010 (2016).
58. M. J. Frisch *et al*., *Gaussian 09 Revision A.01, 2009* (Gaussian Inc., Wallingford, CT, 2009).
59. L. F. Shampine, M. W. Reichelt, The MATLAB ode suite. *SIAM J. Sci. Comput.* **18**, 1–22 (1997).